An open-styled dielectric-lined azimuthally periodic circular waveguide for a millimeter wave traveling-wave tube*

Liu Yang(刘 漾), Wei Yan-Yu(魏彦玉)†, Xu Jin(徐 进), Yin Hai-Rong(殷海荣), Yue Ling-Na(岳玲娜), Gong Yu-Bin(宫玉彬), and Wang Wen-Xiang(王文祥)

Vacuum Electronics National Laboratory, School of Physical Electronics, University of Electronic Science and Technology of China, Chengdu 610054*, China*

(Received 2 August 2011; revised manuscript received 19 September 2011)

An open-styled dielectric-lined azimuthally periodic circular waveguide (ODLAP-CW) for a millimeter-wave traveling-wave tube (TWT) is proposed, which is a modified form of a dielectric-lined azimuthally periodic circular waveguide (DLAP-CW). The slow-wave characteristics of the open-styled DLAP-CW are studied by using the spatial harmonics method, which includes normalized phase velocity and interaction impedance. The complicated dispersion equations are numerically solved with MATLAB and the results are in good agreement with the simulation results obtained from HFSS. The influence of structural parameters on the RF properties is investigated based on our theory. The numerical results show that the optimal thickness of the metal rod can increase the interaction impedance, with the dielectric constant held fixed. Finally, the slow-wave characteristics and transmission properties of an open-styled structure are compared with those of the DLAP-CW. The results validate that the mode competition is eliminated in the improved structure with only a slight influence on the dispersion characteristics, which may significantly improve the stability of an open-styled DLAP-CW-based TWT, and the interaction efficiency is also improved.

Keywords: dispersion characteristics, slow-wave structure, millimeter wave traveling-wave tube, spatial harmonics method

PACS: 84.47.+w, 41.20.Jb, 84.40.Fe **DOI:** 10.1088/1674-1056/21/4/048403

1. Introduction

As an essential component of slow-wave interaction between the electron beam and the RF wave of a traveling-wave tube (TWT), the slow-wave structure (SWS) is a determining factor for the properties of the TWT.[1−5] When the operating frequency increases to the millimeter-wave range, the output power of a TWT based on a conventional SWS such as a helix and a coupled cavity decreases significantly due to beam-current density limitation, thermal-mechanical stability and fabrication issues.[6,7] For these reasons, efforts have been made to develop novel SWSs[8−10] which are characterized by large beam apertures, excellent thermal dissipation properties, and simple structures.

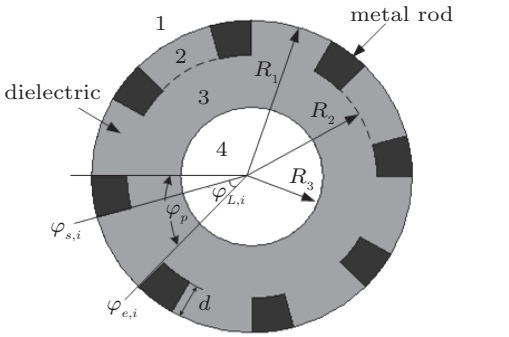
The dielectric-lined azimuthally periodic circular waveguide (DLAP-CW) is regarded as potential SWS for high-power TWT at millimeter-wave and THz frequencies, which has a large beam aperture, high manufacturing precision, and other special characteristics.[11] However, this structure is an over-moded interaction circuit and the operating mode is TM_{01}, not the fundamental mode. Although the results obtained by a previous investigation[11] showed that the interaction impedances of the competing modes are much lower than that of TM_{01}, which indicates a low risk of competing interaction or oscillation, care must be taken when designing the RF circuit. This is because in the beam-wave interaction, the stability of the traveling-wave tube circuit may be influenced by the competing modes. The interaction impedances of competing modes should be as small as possible. Thus, in an effort to alleviate this disadvantage, an improved slow-wave structure, an open-styled dielectric-lined azimuthally periodic circular waveguide (open-styled DLAP-CW) which is a modified form of a DLAP-CW, is proposed in this paper. The difference between the two structures is that the metal shell is removed in the novel structure. The configuration of the open-styled DLAP-CW is shown in Figs. 1(a) and 1(b). The proposed open-styled structure can effectively eliminate the mode compe-

*Project supported by the National Natural Science Foundation of China (Grant No. 60971038) and the Fundamental Research Funds for the Central Universities, China (Grant Nos. ZYGX2009Z003 and ZYGX2010J054).

†Corresponding author. E-mail: yywei@uestc.edu.cn

© 2012 Chinese Physical Society and IOP Publishing Ltd

tition in the beam-wave interaction. As a result, the TWT interaction efficiency and the stability based on such a structure can be expected to be greatly improved.



(a)



(b)

Fig. 1. Schematic diagram of the open-styled DLAP-CW: (a) cross section of the open-styled DLAP-CW, and (b) three-dimensional (3D) view of the open-styled DLAP-CW.

The rest of the present paper is organized as follows. In Section 2, the RF characteristics of the open-styled DLAP-CW, which include the field expressions, analytic dispersion, and interaction impedance, are studied by using the spatial harmonics method (SHM)[12−17] and the field-matching method with an appropriate eigenfunction expansion. In Section 3, the numerical results from Section 2 are compared with HFSS[18] simulations. Additionally, the numerical calculations are carried out by using our theory to investigate the influences of the structural parameters on slow-wave properties. Using the same structural parameters, a comparison between the open-styled DLAP-CW and the conventional one is also carried out. Section 4 is dedicated to a brief summary and conclusion.

2. Theory

The cross section of open-styled dielectric-lined azimuthally periodic circular waveguide is shown in Fig. 1(a), which can be described in terms of a cylindrical coordinate system (r, φ, z). The structure is divided into four regions for analysis: region 1 ($r > R_1$), region 2 ($R_2 < r < R_1$), region 3 ($R_3 < r < R_2$), and region 4 ($r < R_3$). Here, h is the axial length of the structure, N is the number of metal rods, the thicknesses of which are all represented by d and the angle of wedge $\varphi_{L,i}$ is equal to $\varphi_{e,i} - \varphi_{s,i}$. The structure has $1/N$ azimuthal symmetry, in other words, the angular period φ_p is $2\pi/N$.

2.1. Field expression and boundary conditions

The transverse field components in region 1, region 3, and region 4 can be expressed as a series of longitudinal field components, which is represented as a summation of spatial Bloch components by Floquet theory. The series expression for region 2 has a special form, which is expressed as an infinite sum of the eigen standing waves using Fourier expansion. Omitting $\mathrm{e}^{(\mathrm{j}\omega t - \mathrm{j}\beta z)}$, the field expression for E_z is derived, and the other field expressions can then be derived from E_z. In the subsequent analysis, ω represents the angular RF frequency, β the propagation constant, and ε_r is the relative dielectric constant. In addition, m is the azimuthal mode index, which represents the periodicity of the RF field in the azimuthal direction. Here, the TM_{01} ($m = 0$) mode is the only one considered for the longitudinal interaction between the linear beam and the longitudinal field component E_z. The field expressions of these four regions are as follows: in region 1 ($r > R_1$),

$$E_{1z} = \sum_{n=-\infty}^{+\infty} [A_{1n} K_{k_n^\mathrm{I}}(k_{c1} r)] \exp(\mathrm{j} k_n^\mathrm{I} \varphi), \quad (1a)$$

$$E_{1\varphi} = \frac{-\mathrm{j}\beta}{k_{c1}^2} \cdot \frac{1}{r} \frac{\partial}{\partial \varphi} \boldsymbol{E}_{1z}, \quad (1b)$$

$$E_{1r} = \frac{-\mathrm{j}\beta}{k_{c1}^2} \frac{\partial}{\partial r} \boldsymbol{E}_{1z}, \quad (1c)$$

$$H_{1\varphi} = \frac{-\mathrm{j}\omega\varepsilon_r\varepsilon_0}{k_{c1}^2} \frac{\partial}{\partial r} \boldsymbol{E}_{1z}, \quad (1d)$$

$$H_{1r} = \frac{\mathrm{j}\omega\varepsilon_r\varepsilon_0}{k_{c1}^2} \cdot \frac{1}{r} \frac{\partial}{\partial \varphi} \boldsymbol{E}_{1z}, \quad (1e)$$

in region 2 ($R_2 < r < R_1$),

$$E_{2z,i} = \sum_{l=1}^{+\infty} [A_{l,i} J_{k_{l,i}}(k_{c2} r) + B_{l,i} Y_{k_{l,i}}(k_{c2} r)] \times \sin[k_{l,i}(\varphi - \varphi_{s,i})]; \quad (2)$$

in region 3 ($R_3 < r < R_2$),

$$E_{3z} = \sum_{n=-\infty}^{+\infty} [A_{3n} J_{k_n^\mathrm{III}}(k_{c3} r) + B_{3n} Y_{k_n^\mathrm{III}}(k_{c3} r)] \times \exp(\mathrm{j} k_n^\mathrm{III} \varphi); \quad (3)$$

in region 4 ($r < R_3$),

$$E_{4z} = \sum_{n=-\infty}^{+\infty} [A_{4n} I_{k_n^{\mathrm{IV}}}(k_{c4} r) + B_{4n} K_{k_n^{\mathrm{IV}}}(k_{c4} r)] \times \exp(\mathrm{j} k_n^{\mathrm{IV}} \varphi). \quad (4)$$

2.2. Dispersion equation

In order to obtain the equations for the slow-wave characteristics in the analytical model, we use the following boundary and matching conditions of fields at the boundaries between regions.

The tangential components of the electric field are continuous at $r = R_1$, $r = R_2$, and $r = R_3$, therefore

$$\sum_{i=1}^{N} \int_{\varphi_{s,i}}^{\varphi_{e,i}} E_{2z,i}|_{r=R_1} \mathrm{d}\varphi = \int_0^{2\pi} E_{1z}|_{r=R_1} \mathrm{d}\varphi, \quad (5)$$

$$\sum_{i=1}^{N} \int_{\varphi_{s,i}}^{\varphi_{e,i}} E_{2z,i}|_{r=R_2} \mathrm{d}\varphi = \int_0^{2\pi} E_{3z}|_{r=R_2} \mathrm{d}\varphi, \quad (6)$$

$$E_{3z}|_{r=R_3} = E_{4z}|_{r=R_3}. \quad (7)$$

The tangential components of the magnetic field are continuous at $r = R_1$, $r = R_2$, and $r = R_3$, therefore

$$\int_{\varphi_{s,i}}^{\varphi_{e,i}} H_{2\varphi,i}|_{r=R_1} \mathrm{d}\varphi = \int_{\varphi_{s,i}}^{\varphi_{e,i}} H_{1\varphi}|_{r=R_1} \mathrm{d}\varphi, \quad (8)$$

$$\int_{\varphi_{s,i}}^{\varphi_{e,i}} H_{2\varphi,i}|_{r=R_2} \mathrm{d}\varphi = \int_{\varphi_{s,i}}^{\varphi_{e,i}} H_{3\varphi}|_{r=R_2} \mathrm{d}\varphi, \quad (9)$$

$$H_{3\varphi}|_{r=R_3} = H_{4\varphi}|_{r=R_3}. \quad (10)$$

Inserting Eqs. (1)–(4) into the boundary conditions (5)–(10) to eliminate the amplitude constants, the dispersion relation can be written as the following expression:

$$\mathrm{Det} \begin{bmatrix} C_{nq} & 0 & 0 & 0 \\ 0 & D_{nq} & E_{nq} & 0 \\ 0 & F_n & G_n & H_n \\ 0 & M_n & N_n & Q_n \end{bmatrix} = 0, \quad (11)$$

where

$$C_{nq} = \sum_{l=1}^{+\infty} \sum_{i=1}^{N} \Big\{ \sum_{q=-\infty}^{+\infty} K_{k_q^{\mathrm{I}}}(k_{c1} R_1) R(k_q^{\mathrm{I}}, k_l^i) R(-k_n^{\mathrm{I}}, k_l^i) \frac{2}{\varphi_{L,i}} \Big\} - 2\pi \delta_{nq} K_{k_n^{\mathrm{I}}}(k_{c1} R_1),$$

$$D_{nq} = \sum_{l=1}^{+\infty} \sum_{i=1}^{N} \Big\{ \sum_{q=-\infty}^{+\infty} J_{k_q^{\mathrm{III}}}(k_{c2} R_2) R(k_q^{\mathrm{III}} k_l^i) R(-k_n^{\mathrm{III}}, k_l^i) \frac{2}{\varphi_{L,i}} \Big\} - 2\pi \delta_{nq} J_{k_n^{\mathrm{III}}}(k_{c2} R_2),$$

$$E_{nq} = \sum_{l=1}^{+\infty} \sum_{i=1}^{N} \Big\{ \sum_{q=-\infty}^{+\infty} Y_{k_q^{\mathrm{III}}}(k_{c2} R_2) R(k_q^{\mathrm{III}}, k_l^i) R(-k_n^{\mathrm{III}}, k_l^i) \frac{2}{\varphi_{L,i}} \Big\} - 2\pi \delta_{nq} Y_{k_n^{\mathrm{III}}}(k_{c2} R_2),$$

$$F_n = J_{k_n^{\mathrm{III}}}(k_{c2} R_3), \quad G_n = Y_{k_q^{\mathrm{III}}}(k_{c2} R_3), \quad H_n = -I_{k_n^{\mathrm{IV}}}(k_{c4} R_3),$$

$$M_n = \varepsilon_r \varepsilon_0 k_{c4} J'_{k_n^{\mathrm{III}}}(k_{c2} R_3), \quad N_n = \varepsilon_r \varepsilon_0 k_{c4} Y'_{k_n^{\mathrm{III}}}(k_{c2} R_3), \quad Q_n = -\varepsilon_0 k_{c2} I'_{k_n^{\mathrm{IV}}}(k_{c4} R_3).$$

2.3. Interaction Impedance

The interaction impedance of the TM_{0n} mode is defined as

$$K_c = \frac{E_{zn} \cdot E_{zn}^*}{2\beta_n^2 P} = \frac{[A_{4n} I_{k_n^{\mathrm{IV}}}(k_{c4} R_{\mathrm{beam}})]^2}{2\beta_n^2 \Big(\sum\limits_{n=-\infty}^{+\infty} P_1 + \sum\limits_{l=1}^{+\infty} P_2 + \sum\limits_{n=-\infty}^{+\infty} P_3 + \sum\limits_{n=-\infty}^{+\infty} P_4 \Big)}, \quad (12)$$

where E_{zn} is the longitudinal electric field of the n-th space harmonic, E_{zn}^* is its conjugate, β_n is the axial wavenumber of the n-th space harmonic, and P is the total power flow in the z direction (axial power flow). The axial power flows through each region are obtained as

$$P_1 = A_{1n}^2 \cdot \frac{\omega \beta \varepsilon_0}{2k_{c1}^2} \Big\{ \int_{R_1}^{+\infty} \int_0^{2\pi} [K'_{k_n^{\mathrm{I}}}(k_{c1} r)]^2 r \mathrm{d}r \mathrm{d}\varphi + \frac{(k_n^{\mathrm{I}})^2}{k_{c1}^2} \int_{R_1}^{+\infty_1} \int_0^{2\pi} [K_{k_n^{\mathrm{I}}}(k_{c1} r)]^2 \frac{1}{r} \mathrm{d}\varphi \mathrm{d}r \Big\},$$

$$P_2 = \frac{\omega \beta \varepsilon_r \varepsilon_0}{2k_{c2}^2} \sum_{i=1}^{+\infty} \Big\{ \int_{R_2}^{R_1} \int_{\varphi_{s,i}}^{\varphi_{e,i}} [A_{l,i} J'_{k_{l,i}}(k_{c2} r) + B_{l,i} Y'_{k_{l,i}}(k_{c2} r)]^2 \sin^2[k_{l,i}(\varphi - \varphi_{s,i})] r \mathrm{d}r \mathrm{d}\varphi$$
$$+ \frac{(k_l^i)^2}{k_{c2}^2} \int_{R_2}^{R_1} \int_{\varphi_{s,i}}^{\varphi_{e,i}} [A_{l,i} J_{k_{l,i}}(k_{c2} r) + B_{l,i} Y_{k_{l,i}}(k_{c2} r)]^2 \cos^2[k_{l,i}(\varphi - \varphi_{s,i})]^2 \frac{1}{r} \mathrm{d}\varphi \mathrm{d}r \Big\},$$

$$P_3 = \frac{\omega \beta \varepsilon_r \varepsilon_0}{2k_{c2}^2} \Big\{ \int_{R_3}^{R_2} \int_0^{2\pi} [A_{3n} J'_{k_n^{\mathrm{III}}}(k_{c2} r) + B_{3n} Y'_{k_n^{\mathrm{III}}}(k_{c2} r)]^2 r \mathrm{d}r \mathrm{d}\varphi$$

$$+\frac{(k_n^{\mathrm{III}})^2}{k_{c2}^2}\int_{R_3}^{R_2}\int_0^{2\pi}[A_{3n}J_{k_n^{\mathrm{III}}}(k_{c2}r)+B_{3n}Y_{k_n^{\mathrm{III}}}(k_{c2}r)]^2\frac{1}{r}\mathrm{d}\varphi\mathrm{d}r\Big\},$$

$$P_4=A_{4n}^2\cdot\frac{\omega\beta\varepsilon_0}{2k_{c4}^2}\Big\{\int_0^{R_3}\int_0^{2\pi}[I'_{k_n^{\mathrm{IV}}}(k_{c4}r)]^2r\,\mathrm{d}r\,\mathrm{d}\varphi+\frac{(k_n^{\mathrm{IV}})^2}{k_{c4}^2}\int_0^{R_3}\int_0^{2\pi}[I_{k_n^{\mathrm{IV}}}(k_{c4}r)]^2\frac{1}{r}\mathrm{d}\varphi\mathrm{d}r\Big\},$$

where P_1, P_2, P_3, and P_4 are the axial power flows through region 1, region 2, region 3, and region 4, respectively. The relative values of A_{1n}, $A_{l,i}$, $B_{l,i}$, A_{3n}, B_{3n}, and A_{4n} can be obtained by solving Eq. (12), and the results are

$$B_{l,i}=\frac{\frac{k_{c2}}{k_{c1}\varepsilon_r}\sum_n A_{1n}K'_{k_n^{\mathrm{I}}}(k_{c1}R_1)R(k_n^{\mathrm{I}},k_{l,i})J_{k_{l,i}}(k_{c2}R_1)-\sum_n A_{1n}K_{k_n^{\mathrm{I}}}(k_{c1}R_1)J'_{k_{l,i}}(k_{c2}R_1)}{\frac{\varphi_{L,i}}{2}[J_{k_{l,i}}(k_{c2}R_1)Y'_{k_{l,i}}(k_{c2}R_1)-J'_{k_{l,i}}(k_{c2}R_1)Y_{k_{l,i}}(k_{c2}R_1)]},$$

$$A_{l,i}=\frac{\frac{2}{\varphi_{L,i}}\sum_n A_{1n}K_{k_n^{\mathrm{I}}}(k_{c1}R_1)R(k_n^{\mathrm{I}},k_{l,i})-B_{l,i}Y_{k_{l.i}}(k_{c2}R_1)}{J_{k_{l.i}}(k_{c2}R_1)},$$

$$R(-k_n^{\mathrm{I}},k_{l,i})=\int_{\varphi_{s,i}}^{\varphi_{e,i}}\sin[k_{l,i}(\varphi-\varphi_{s,i})]\exp(-jk_n^{\mathrm{I}}\varphi)\mathrm{d}\varphi,$$

$$R(k_q^{\mathrm{I}},k_{l,i})=\int_{\varphi_{s,i}}^{\varphi_{e,i}}\sin[k_{l,i}(\varphi-\varphi_{s,i})]\exp(jk_q^{\mathrm{I}}\varphi)\mathrm{d}\varphi,$$

$$X_1=\sum_{l=1}^{+\infty}\sum_{i=1}^{N}[A_{l,i}J_{k_{l,i}}(k_{c2}R_2)+B_{l,i}Y_{k_{l,i}}(k_{c2}R_2)]R(-k_n^{\mathrm{I}},k_{l,i}),$$

$$X_2=\sum_{l=1}^{+\infty}\sum_{i=1}^{N}[A_{l,i}J'_{k_{l,i}}(k_{c2}R_2)+B_{l,i}Y'_{k_{l,i}}(k_{c2}R_2)]R(-k_n^{\mathrm{I}},k_{l,i}),$$

$$B_{3n}=\frac{J'_{k_n^3}(k_{c2}R_2)X1-J_{k_n^3}(k_{c2}R_2)X2}{2\pi\Big[J'_{k_n^3}(k_{c2}R_2)Y_{k_n^3}(k_{c2}R_2)-J_{k_n^3}(k_{c2}R_2)Y'_{k_n^3}(k_{c2}R_2)\Big]},$$

$$A_{3n}=\frac{X1-2\pi B_{3n}Y_{k_n^3}(k_{c2}R_2)}{2\pi\Big[J'_{k_n^3}(k_{c2}R_2)Y_{k_n^3}(k_{c2}R_2)-J_{k_n^3}(k_{c2}R_2)Y'_{k_n^3}(k_{c2}R_2)\Big]},$$

$$A_{4n}=\frac{A_{3n}J_{k_n^{\mathrm{III}}}(k_{c2}R_3)+B_{3n}Y_{k_n^{\mathrm{III}}}(k_{c2}R_3)}{I_{k_n^{\mathrm{IV}}}(k_{c4}R_3)}. \tag{13}$$

Using the results of the dispersion relation obtained in Section 3, and substituting Eq. (13) into Eq. (12), the interaction impedance of the open-styled DLAP-CW is obtained.

3. Numerical results and discussion

The dispersion equation (11) and the interaction impedance equation (12) can be solved numerically using the Matlab[19] computer software package. For comparison, we simulated the structure using a three-dimensional (3D) electromagnetic code HFSS in order to verify the correctness of the present theory. The results of the open-styled DLAP-CW with $\varepsilon=10$, $R_1/R_3=2$, $R_2/R_3=1.5$, $\varphi_{L,i}=\pi/6$, $N=8$, and $R_3=2$ mm in Fig. 2 indicate that the HFSS simulation data accord well with the numerical calculation data obtained from the present theory, which supports our theory. Next we investigate the effects of the structural parameters on the slow-wave properties of the open-styled dielectric-lined azimuthally periodic circular waveguide according to our theory.

Figure 3(a) shows the effect of the dielectric constant on the normalized phase velocity of the open-styled DLAP-CW. It can be concluded that with the increase of ε the relative passband becomes wide and the phase velocity decreases. At the same time, the cutoff frequency decreases and the passband range shifts toward lower frequency.

Meanwhile, the interaction impedance versus normalized frequency for the open-styled DLAP-CW with the variation of the dielectric constant ε is investigated in Fig. 3(b). The results show that the interaction impedance increases noticeably with the decrease of the dielectric constant ε. On the other hand, if choosing a material with a small dielectric constant ε, the normalized phase velocity will become too high. In other words, its high phase velocity indicates that the TWT based on such a structure needs a relatively

high operating voltage for satisfying the synchronous conditions in the beam-wave interaction, which may restrict the further application in the compact TWT interaction circuits.

The normalized phase velocities and the interaction impedances for several thicknesses of the metal rods versus frequency are plotted with ε fixed at 12, respectively, in Fig. 4 (a) and Fig. 4 (b). The normalized phase velocity decreases as the thickness of the metal rod, d, decreases. At the same time, the dispersion curve also becomes steeper. And the interaction impedance first increases but then decreases as the thickness d increases. Therefore, the thickness of the metal rod for a specific open-styled DLAP-CW design must be carefully optimized to improve the performance of the beam-wave interaction in an open-styled DLAP-CW-based TWT. Here, curve B in Fig. 4(b) indicates that the interaction impedance of the open-styled DLAP-CW with $d = 1$ mm is optimal.

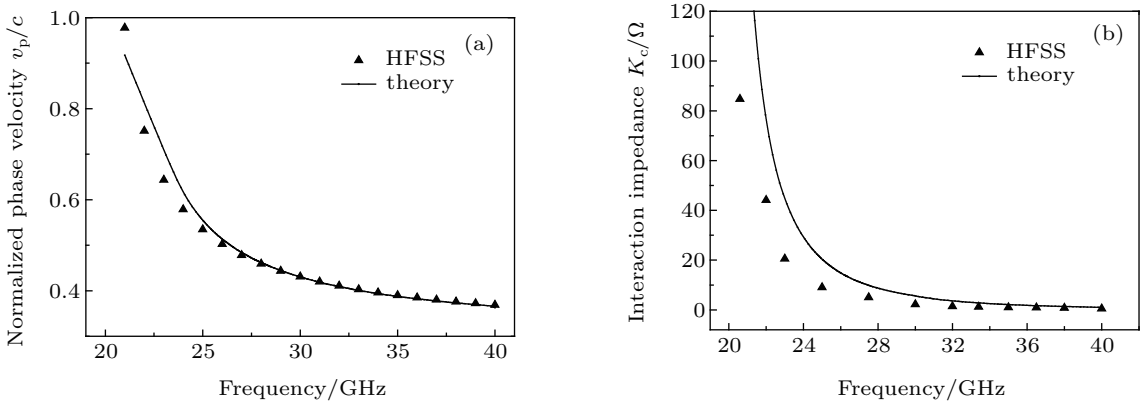


Fig. 2. Dispersion curves of open-styled DLAP-CW: (a) normalized phase velocity and (b) interaction impedance of open-styled DLAP-CW, calculated using the present theory and HFSS.

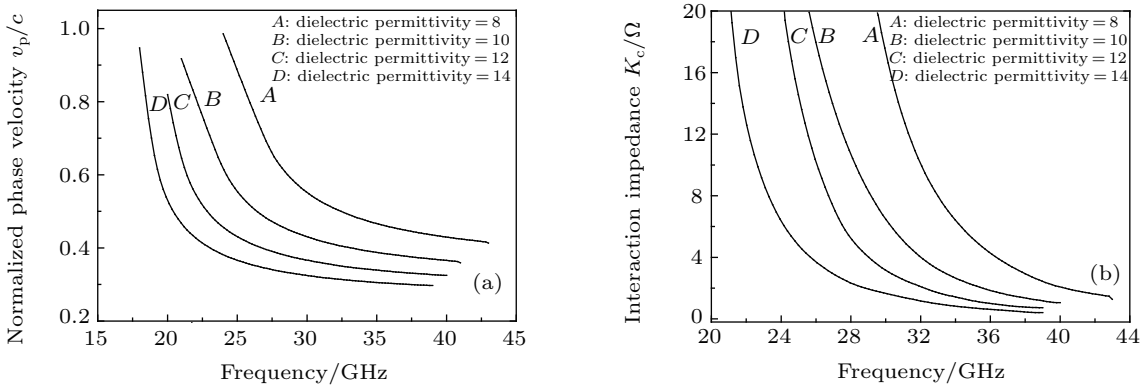


Fig. 3. Dispersion characteristics for some different dielectric constants when $R_1/R_3 = 2$, $R_2/R_3 = 1.5$, $\varphi_{L,i} = \pi/6$, $N = 8$, and $R_3 = 2$ mm: (a) normalized phase velocity and (b) interaction impedance.

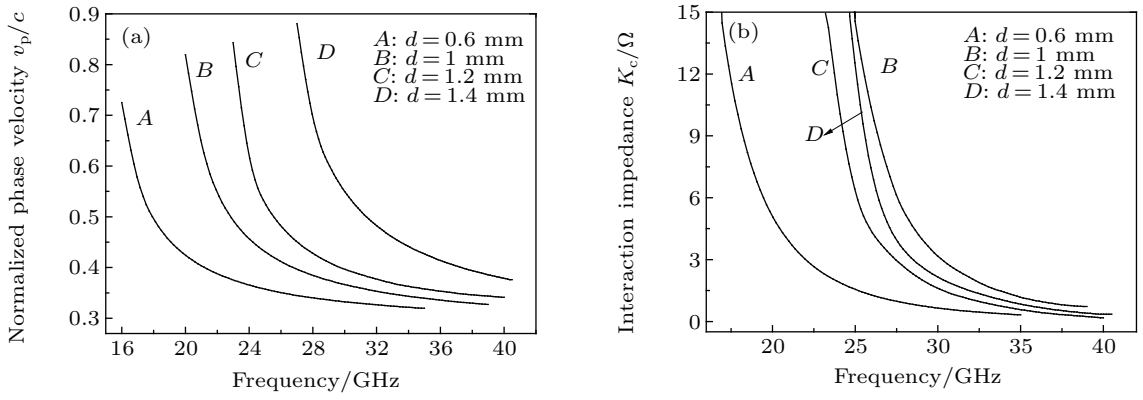


Fig. 4. Dispersion characteristics for some different values of d when $\varepsilon = 12$, $R_1/R_3 = 2$, $\varphi_{L,i} = \pi/6$, $N = 8$, and $R_3 = 2$ mm: (a) normalized phase velocity, and (b) interaction impedance.

Finally, we investigate the slow-wave characteristics and the transmission properties of a DLAP-CW and an open-styled DLAP-CW with the same dimensions. The results obtained from the present theory in Fig. 5 show that the interaction impedance of the ODLAP-CW slightly increases compared with that of DLAP-CW when the dispersion characteristics are similar. Furthermore, compared with a DLAP-CW in the same case, the results in Figs. 6 and 7 from full 3D simulations using HFSS show that the values of transmission coefficient $S12$ of the competing modes are all less than -12 dB, and that of the operating mode is close to 0 dB in the open-styled DLAP-CW while there is little influence of the reflection coefficient $S11$. This indicates that the mode competition will be eliminated in the beam-wave interaction. In other words, there is a significant improvement on the stability of an open-styled DLAP-CW-based TWT, and the interaction efficiency is also improved.

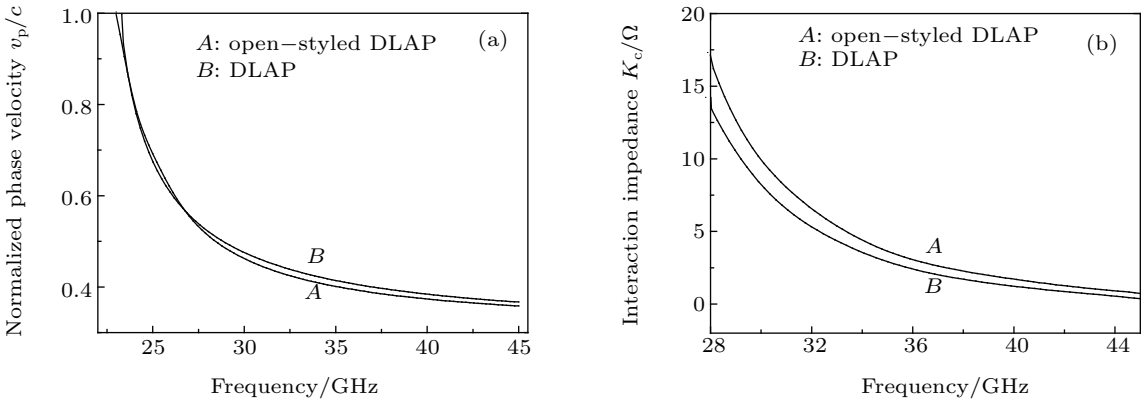


Fig. 5. Comparison of the dispersion characteristic between open-styled DLAP-CW and DLAP-CW with $\varepsilon = 10$, $R_1/R_3 = 2$, $R_2/R_3 = 1.5$, $\varphi_{L,i} = \pi/9$, $N = 8$, and $R_3 = 2$ mm: (a) normalized phase velocity and (b) interaction impedance.

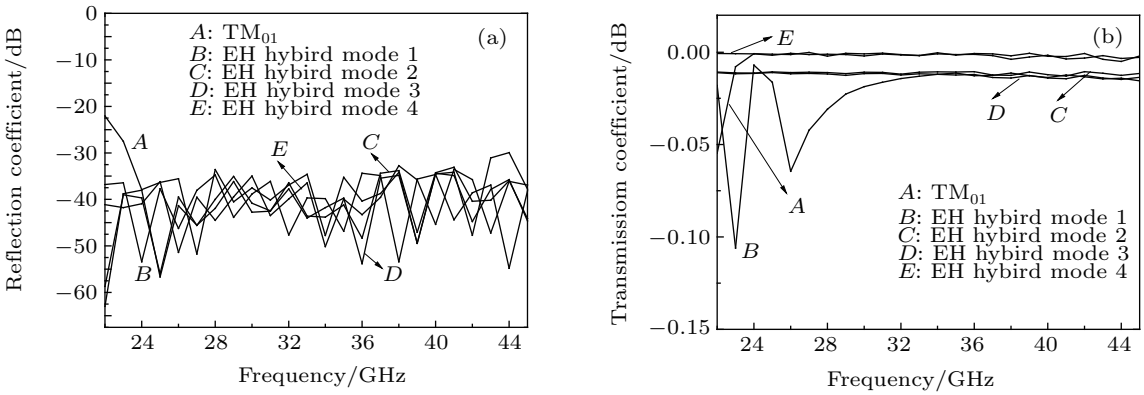


Fig. 6. Transmission properties for DLAP-CW: (a) reflection coefficient $S11$ and (b) transmission coefficient $S12$.

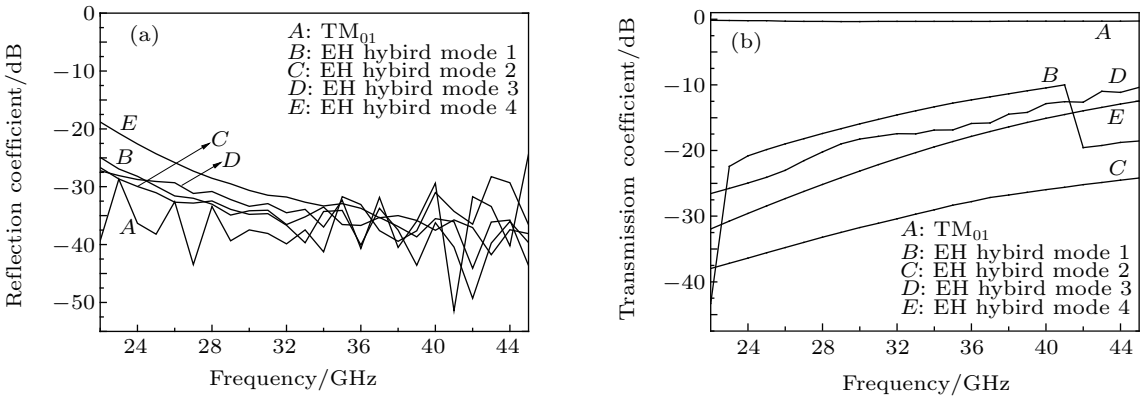


Fig. 7. Transmission properties for open-styled DLAP-CW: (a) reflection coefficient $S11$ and (b) transmission coefficient $S12$.

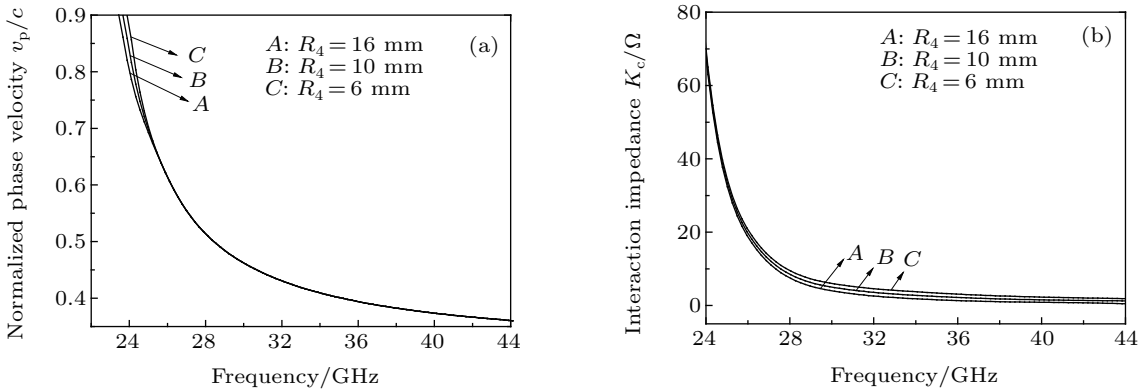


Fig. 8. Dispersion characteristics for some different values of R_4 when $\varepsilon = 10$, $R_1/R_3 = 2$, $\varphi_{L,i} = \pi/9$, $N = 8$, and $R_3 = 2$ mm: (a) normalized phase velocity and (b) interaction impedance.

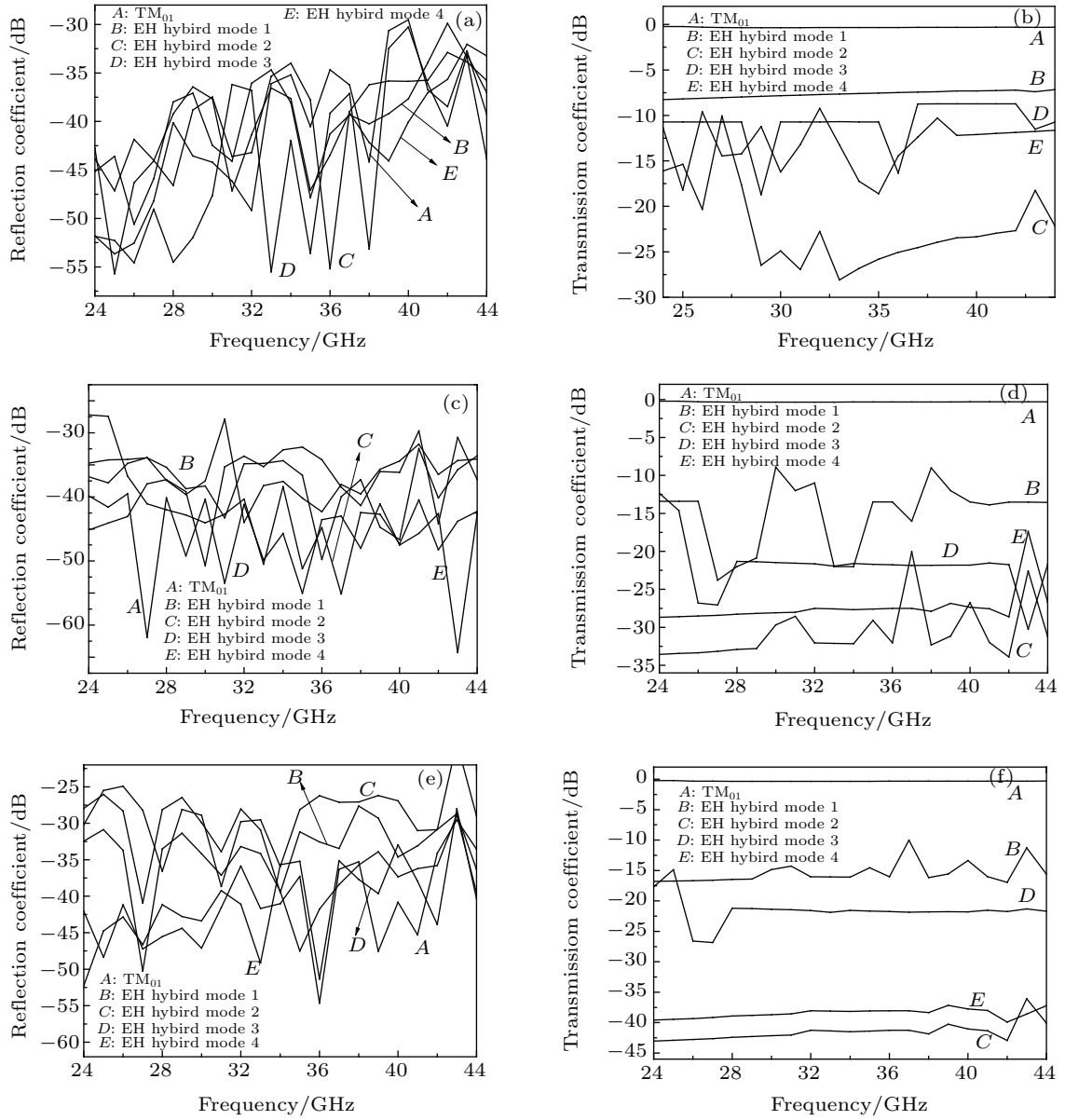


Fig. 9. Transmission properties for some different values of R_4: (a) reflection coefficient $S11$ and (b) transmission coefficient $S12$ ($R_4 = 6$ mm); (c) reflection coefficient $S11$ and (d) transmission coefficient $S12$ ($R_4 = 10$ mm); (e) reflection coefficient $S11$ and (f) transmission coefficient $S12$ ($R_4 = 16$ mm).

Meanwhile, a new magnetic focusing system structure is needed in practical applications, which may affect the open style of this structure. As a result, the performance of the ODLAP-CW is studied when the focusing system is considered. In the following research, the inner wall of the pole shoes of the period permanent magnet (PPM) focusing system is replaced by a metal boundary in order to make analysis convenient, and the radius of the metal shell is represented by R_4. The influences of radius R_4 on the RF properties are indicated in Figs. 8 and 9, obtained by the HFSS simulation, which include the dispersion characteristics, the interaction impedances, and the transmission properties.

From Fig. 8 it follows that for the R_4 values of 6, 10, and 16 mm, the normalization phase velocity and the interaction impedance for TM_{01} mode vary little with frequency. Furthermore, in Fig. 9, it is clear that as radius R_4 increases, the competing modes cannot transport well expect the operation mode TM_{01}, which is close to that of an open-styled structure in this case. At the same time, the inhibition of the mode competition is rapidly enhanced, which is the advantage of the ODLAP-CW.

In practical applications, the ODLAP-CW needs a magnetic focusing system in order to achieve a stable and nonintercepting transmission of the electronic beam in this structure. In addition, it is good for the open style of this structure when a large radius R_4 is chosen, thereby increasing size and weight of the focusing system, which is unacceptable for linear beam TWT interaction circuits. For these reasons, attenuators are loaded between the slow-wave structure and the focusing system, or a layer of attenuating material is evaporated on the structure, which can effectively attenuate the energy of the competing modes without deteriorating the transmission properties of the operating mode TM_{01}. This is because the electric field energy of the operation mode is concentrated mainly in the electron beam channel, and the field energies of the other competitive modes are distributed at the edge of the structure.

4. Conclusion

In this paper, the equations for the slow-wave characteristics including phase velocity and interaction impedance of the open-styled dielectric-lined azimuthally periodic circular waveguide (open-styled DLAP-CW) are derived using a spatial harmonics method. The theoretical solutions are well consistent with the results from full 3D simulations using HFSS, which supports our theory. Furthermore, the effect of the SWS dimension on the RF characteristics of this circuit and the parametric analysis reveal that the dielectric constant and the thickness of the metal rod both significantly influence the open-styled DLAP-CW characteristics. Consequently, it is necessary to select optimal structural parameters to strike a balance between the bandwidth and the interaction impedance. Finally, we compare the transmission characteristics and RF properties between a DLAP-CW and an open-styled DLAP-CW with same structural dimensions. The results show that the interaction impedance of the open-styled DLAP-CW slightly increases when their dispersion characteristics are similar. In the open-styled DLAP-CW, the mode competition is eliminated in the beam-wave interaction. Therefore, there is a significant improvement in the stability of an open-styled DLAP-CW-based TWT, and the interaction efficiency is also improved.

References

[1] Menninger W L, Robbins N R and Dibb D E 2007 *IEEE Trans. Electron Dev.* **54** 181

[2] Gong Y B, Wei Y Y and Huang M Z 2008 *GMSS* 978

[3] Lu Z G, Gong Y B, Wei Y Y and Wang W X 2006 *Chin. Phys.* **15** 2661

[4] Chong C K, Davis J A and Le Brogn R H 2005 *IEEE Trans. Electron Dev.* **52** 653

[5] Legarra J R, Kolda P E and Freund H P 2002 *IEEE MTT-s Digest* 625

[6] He J, Wei Y Y, Gong Y B and Wang W X 2009 *Chin. Phys. Lett.* **26** 114103

[7] Wei Y Y, Wang W X, Sun J H, Liu S G, Jia B F and Park Gun-Sik 2002 *Chin. Phys.* **11** 277

[8] He J, Wei Y Y, Gong Y B and Wang W X 2011 *Chin. Phys.* B **20** 054102

[9] Xu A, Wang W X, Wei Y Y, Gong Y B, Wang Z L, Fu C F and Yin H R 2009 *Acta Phys. Sin.* **58** 3592 (in Chinese)

[10] He J, Wei Y Y, Gong Y B, Duan Z Y and Wang W X 2010 *Acta Phys. Sin.* **59** 2843 (in Chinese)

[11] Liu Y, Wei Y Y, Gong Y B and Wang W X 2010 *IEEE Trans. Electron Dev.* **57** 2019

[12] Collin R E 1960 *Field Theory of Guided Waves* (New York: McGraw-Hill) Chap. 11

[13] Ioannidis Z C, Dumbrajs O and Tigelis I G 2004 *IEEE Trans. Plasma Sci.* **32** 861

[14] Ioannidis Z C, Latas G P and Tigelis I G 2008 *IEEE Trans. Plasma Sci.* **36** 2613

[15] Iatrou C T, Kern S and Pavelyev A B 1996 *IEEE Trans. Microwave Theory Tech.* **44** 56

[16] Fu C F, Wei Y Y, Duan Z Y, Wang W X and Gong Y B 2009 *Chin. Phys.* **18** 2749

[17] He J, Wei Y Y, Gong Y B, Duan Z Y, Lu Z G and Wang W X 2010 *Acta Phys. Sin.* **59** 6659 (in Chinese)

[18] AnosftCorp. 2001 (more information available online: http://www.ansoft.com/)

[19] Mathworks. Inc., Natick, Massachusetts 2004 (more information available online: http://www.mathworks.com/)